ACS APPLIED MATERIALS & INTERFACES

Research Article

www.acsami.org

# Cell-Imprinted Substrates Act as an Artificial Niche for Skin Regeneration

Omid Mashinchian,[†] Shahin Bonakdar,[‡] Hossein Taghinejad,[∥] Vahid Satarifard,[⊥] Maziar Heidari,[#,∇] Mohammad Majidi,[‡] Shahriar Sharifi,[○] Afshin Peirovi,[§] Samaneh Saffar,[§] Mohammad Taghinejad,[∥] Mohammad Abdolahad,[∥] Shams Mohajerzadeh,[∥] Mohammad Ali Shokrgozar,[‡] Seyed Mahdi Rezayat,[†] Mohammad R. Ejtehadi,[◆] Matthew J. Dalby,[¶] and Morteza Mahmoudi*[,▲,□]

[†]Department of Medical Nanotechnology, School of Advanced Technologies in Medicine (SATiM), Tehran University of Medical Sciences, P.O. Box 14177-55469, Tehran, Iran

[‡]National Cell Bank and [§]Core Facility Center, Pasteur Institute of Iran, P.O. Box 13169-43551, Tehran, Iran

[∥]Nanoelectronic Center of Excellence, Thin Film and Nanoelectronic Lab, School of Electrical and Computer Engineering, University of Tehran, P.O. Box 14395/515, Tehran, Iran

[⊥]School of Chemistry, College of Science, University of Tehran, P.O. Box 14155-6455, Tehran, Iran

[#]School of Mathematics, Institute for Research in Fundamental Sciences (IPM), P.O. Box 19395-5746, Tehran, Iran

[∇]Department of Mechanical Engineering, Sharif University of Technology, P.O. Box 11365-9567, Tehran, Iran

[○]MIRA Institute for Biomedical Technology and Technical Medicine, Department of Biomaterials Science and Technology, University of Twente, P.O. Box 217, 7500 AE, Enschede, The Netherlands

[◆]Department of Physics, Sharif University of Technology, P.O. Box 11155-9161, Tehran, Iran

[¶]Centre for Cell Engineering, Institute of Biomedical and Life Sciences, University of Glasgow, Joseph Black Building, Glasgow G12 8QQ, Scotland

[▲]Department of Nanotechnology & Nanotechnology Research Center, Faculty of Pharmacy, Tehran University of Medical Sciences, P.O. Box 14155-6451, Tehran, Iran

Supporting Information

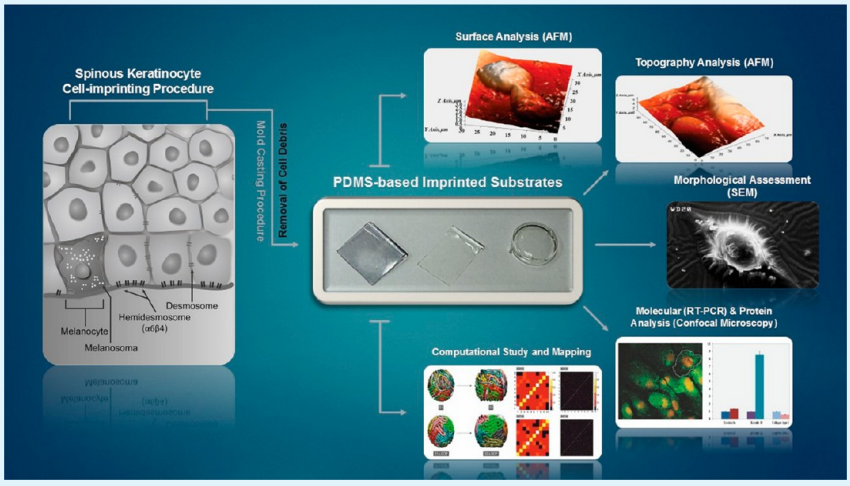


**ABSTRACT:** Bioinspired materials can mimic the stem cell environment and modulate stem cell differentiation and proliferation. In this study, biomimetic micro/nanoenvironments were fabricated by cell-imprinted substrates based on mature human keratinocyte morphological templates. The data obtained from atomic force microscopy and field emission scanning electron microscopy revealed that the keratinocyte-cell-imprinted poly(dimethylsiloxane) casting procedure could imitate the surface morphology of the plasma membrane, ranging from the nanoscale to the macroscale, which may provide the required topographical cell fingerprints to induce differentiation. Gene expression levels of the genes analyzed (involucrin, collagen type I, and keratin 10)
*continued...*

**Received:** May 21, 2014
**Accepted:** June 26, 2014
**Published:** June 26, 2014

  

together with protein expression data showed that human adipose-derived stem cells (ADSCs) seeded on these cell-imprinted substrates were driven to adopt the specific shape and characteristics of keratinocytes. The observed morphology of the ADSCs grown on the keratinocyte casts was noticeably different from that of stem cells cultivated on the stem-cell-imprinted substrates. Since the shape and geometry of the nucleus could potentially alter the gene expression, we used molecular dynamics to probe the effect of the confining geometry on the chain arrangement of simulated chromatin fibers in the nuclei. The results obtained suggested that induction of mature cell shapes onto stem cells can influence nucleus deformation of the stem cells followed by regulation of target genes. This might pave the way for a reliable, efficient, and cheap approach of controlling stem cell differentiation toward skin cells for wound healing applications.

KEYWORDS: *nanotopography, stem cell, differentiation, smart substrate, niche, chromatin fibers, geometry, cell morphology*

## 1. INTRODUCTION

Stem cells (SCs) have the potential to underpin a diverse range of applications in advanced regenerative medicine and biopharmaceutical sciences.[1,2] The natural regeneration and development procedure in the human body is performed by multipotent cells, which control specific interactions with various biochemicals, as well as physical cues in their extracellular matrix (ECM).[3−5] In this regard, the ECM applies powerful control over numerous cellular/molecular phenomena, such as regulation of stem cell differentiation.[6] Typically, control of the phenotypical expression and function of stem cells either in vivo or in vitro is regulated by their integrated response to various biochemical cues, such as growth factors, cytokines, and/or cell−cell interactions. In the complex microenvironment, cells encounter a multitude of distinct, active stimuli that are biochemical, structural, and mechanical in nature. Similarly to biochemical cues, such physical cues can also affect diverse cell response.[7−9] For instance, recent developments have confirmed that matrix-mediated signals, such as the surface composition, surface-adhesive ligands, the surface topography, and the shear stress of the medium, have a profound impact on stem cell behavior such as proliferation, migration, and differentiation.[4,10−13]

New insights into the complete regulation of self-renewal and differentiation of stem cells could be achieved by understanding the exact interaction of these novel mediators with cell signaling pathways. For instance, structural cues such as the substrate topography can strongly influence the polarity of many different cell types by contact guidance through cytoskeletal and nucleoskeletal rearrangement.[14]

These changes in subcellular structures are correlated with changes in the gene expression profile and cell differentiation.[15] As the native ECM likely comprises nanoscale topography within the stem cell niche, micro- and nanopatterned substrates (which are typically created by microcontact printing and photo/electron beam lithography patterning methods) are recognized as the most commonly used biomaterials to study the effects of cell culture topography on the stem cell fate.[16,17] For instance, nanotopography has even been linked to potential MSC transdifferentiation toward neural lineages.[18]

In addition, nanotopography provides a useful and noninvasive platform for studying the effects of mechanotransduction. Mechanotransduction, the specific mechanism by which cells convert physical cues (e.g., mechanical forces) into biochemical responses, plays a crucial role in controlling differentiation of stem cells, leading to their commitment into a specific lineage.[19−21] With respect to topography, mechanotransduction applied through rearrangement of adhesions and cytoskeletal networks leads to alterations in intracellular tension and mechanosensitive ion channels.[4] It has also been shown using nanotopography that mechanotransduction can have a strong effect on cell metabolism and metabolic signaling that can feed into biochemical pathways and that this changes from the stem cell growth state[22] to the active differentiation state.[23]

Despite the intense scientific efforts to achieve precise control of stem cell fates with engineered patterned substrates, reliable and cost-effective control of stem cell behavior remains a challenge. As the cell sizes are in the micrometer range while patterns can be created at nanometer resolution, the optimal surface topography for a given cell type and the number of possible surface patterns that can be created are virtually unlimited. Hence, while approaches to control of substrate stiffness (tissue matching) and chemistry (e.g., hydrophilicity) are fairly intuitive,[24] the approach to topography has been, due to the vast number of iterations achievable, rather haphazard with few rules defined.[25] In this context, the ability to prepare a topographically optimized niche microenvironment on cell culture substrates, which can control cell behavior, may further extend our capabilities to manufacture the tissue substitutes, and it may be advantageous to look to nature to achieve this.[9,26−28]

In a former study, we showed that cell imprinting is a promising approach to recapitulate the ECM architecture. It was shown that cell-imprinted surfaces containing "casts" of chondrocyte cell morphologies induced the differentiation of rabbit adipose-derived mesenchymal stem cells (ADSCs) into the chondrocytes when cultured on the casts, i.e., use of bioinspired topography at the micro- and nanolevels.[9]

The skin is a classical example of a tissue supported by stem cells as it must regenerate constantly during normal homeostasis and after being wounded.[29] Therefore, fulfilling these functions demands a specific pool of stem cells to maintain the epidermis. The stem cell niches in skin have long been thought to locate within the basal layer; nevertheless, the role of microenvironmental cues and other sources of growth/lineage-defining signals remains unclear.

In this in vitro study, a 3D surface imitating the morphology of the keratinocyte plasma membrane was used as a biomimetic template for differentiation of ADSCs into keratinocyte-like cells (KLCs). Toward a better understanding of the shape/pattern-induced stem cell differentiation process, molecular dynamic (MD) simulation was performed. In the simulation, the chromatin fibers of the morphologically altered nucleus were modeled as coarse-grained bead−spring polymer chains. The results were correlated with the shape/pattern-induced stem cell differentiation process.

## 2. EXPERIMENTAL SECTION

**2.1. Isolation and Culture of Adipose-Derived Stem Cells.** For this procedure, adipose tissue samples were obtained from liposuction aspirates and needle biopsy according to a previously published methodology.[30] After transportation to the cell culture laboratory, the liposuction samples in Dulbecco's modified Eagle's medium (DMEM; Gibco, Scotland) containing 10% (v/v) fetal bovine serum (FBS) (Seromed, Germany) and penicillin (100 IU/mL)−streptomycin

(100 μg/mL) (Sigma, United States) were kept at room temperature for a maximum of 1 day before use. Prior to the experiments being performed, the cells were washed three times in DMEM-based buffer. Adipose tissues were harvested with an incision and were chopped into small pieces followed by digestion in an incubator with 0.02 mg/mL collagenase type I (Sigma, United States) for a period of 1 h. The suspension obtained was centrifuged at 200*g* for 5 min, and the cell pellets were separated. The sample of ADSCs was transferred to the culture medium consisting of DMEM/Ham's F12 supplemented with 10% FBS, 100 U/mL penicillin, and 100 μg/mL streptomycin in a humidified incubator (37 °C, 5% $CO_2$). After 24 h, nonadhered cells and debris were removed, and new culture medium was added.

**2.2. Isolation and Culture of Human Epidermal Keratinocytes (HKs).** With consent from parents, human epidermis was isolated from the neonatal foreskin at the time of circumcision. The samples were rinsed three times with phosphate-buffered saline (PBS) and sliced into strips using a scalpel. Before working with the samples, they were washed three times in washing solution (DMEM containing penicillin−streptomycin) for removal of probable infection. Subsequently, the samples were incubated in 0.25% trypsin solution at 37 °C for 1 h. After centrifugation at 500*g* for 5 min, the samples were vortexed, and FBS was added to inhibit the digestion effect of the trypsin. The obtained suspension was centrifuged at 500*g* for 5 min, and the cell pellet was resuspended in the fresh culture medium. The cell viability was assessed utilizing trypan blue exclusion. The cells were cultured with keratinocyte growth medium (KGM) with its supplements, including DMEM/Ham's F12 in a 3:1 ratio, 10% (v/v) FBS, epidermal growth factor (EGF; 2 ng/mL), hydrocortisone (0.18 μg/mL), insulin (10 μg/mL), penicillin (100 IU/mL)−streptomycin (100 μg/mL), epinephrine (0.5 μg/mL), and prostaglandin E2 (10 ng/mL) (all from Gibco-BRL, Germany). Additionally, in another experiment, growth-arrested 3T3 mouse embryonic fibroblasts (MEFs) (obtained from the National Cell Bank of Iran (NCBI), Pasteur Institute of Iran, NCBI-C162) were used as a feeder layer to enhance the culture of the keratinocytes in vitro. It is notable that the MEFs were treated with mitomycin C (Sigma) to inhibit their proliferation. For this purpose, 10 μg/mL mitomycin C was used to treat the 3T3 cells at 37 °C for 2−3 h. After the incubation, the cells were rinsed three times with fresh culture medium to remove the mitomycin C.[31]

**2.3. Characterization of HKs.** For detection and characterization of keratinocyte cells, a fluorescence microscope (Axioscope, Zeiss, Germany) was employed. Two common types of monoclonal antibodies (i.e., mouse antihuman involucrin antibody (Abcam, United States) and mouse antihuman pan-keratin antibody (Abcam)) were used for keratinocyte detection. The cells were fixed using 4% formaldehyde (Sigma) for 10−15 min and permeabilized with Triton X-100 (Sigma). After three washes with ice-cold PBS, the primary antibodies were incubated on the cells for 1.5 h, followed by additional incubation with the secondary antibody solution (antimouse−Ig−FITC (Abcam); Ig = immunoglobulin; FITC = fluorescein isothiocyanate) in the dark at room temperature for 1 h.

**2.4. Fabrication Procedure of Cell-Imprinted Substrates.** Poly(dimethylsiloxane) (PDMS; SYLGARD 184, RTV, Dow Corning, United States) was used to fabricate the cell-imprinted substrates. The silicone resin and curing agent were mixed with a 10:1 ratio and then heated for 30−35 min at 45 °C with a digitally controlled microplate heater. A total of 30 × $10^3$ keratinocyte cells and ADSCs were cultured for 24 h according to standard cell culture procedures[32,33] on polystyrene well plates in DMEM/Ham's F12 (in a 3:1 ratio), 10% (v/v) FBS, 100 U/mL penicillin, and 100 μg/mL streptomycin. The cell medium was removed from the plates completely before the next step. After cooling of the preheated elastomer solution to 37 °C, the cured silicone was poured onto each of the cell cultured samples and incubated at 37 °C for 24−48 h before the imprinted substrates were obtained. To have better control of the functional substrates, which can entirely mimic the cell morphology, the cells were fixed with 4% glutaraldehyde before treatment with PDMS to maintain their shape during the printing process. Additionally, to investigate the influence of the substrate surface morphology, the keratinocyte cell culture experiment was designed using three in vitro models: (i) The keratinocyte cells were cultured on 24-well plates which were precoated with collagen type I solution (Sigma) (0.8 mg/mL in 0.1% acetic acid at pH 7.4). It is noteworthy that the cultured cells reached 70% confluency and were ready for passage within 2 weeks. (ii) The keratinocyte−3T3 mouse embryonic fibroblast cells were cultured on six-well plates, noting that keratinocyte cell proliferation can be stimulated by 3T3 cells in coculture. The cultured cells reached 70% confluency and were ready for passage within 10 days. (iii) The keratinocyte cells were cultured on 96-well plates without any feeder layer. Subsequently, the cured silicone was peeled from the cell culture plates in all experiments. This step was followed by numerous washing procedures of the silicone substrates using boiled water and 1 M NaOH solution to remove remaining cells/debris and other chemicals from the substrates. The most important factor for improving the imprinting efficiency is optimization of the curing time and the total mass of the silicone, and in this case the lower thickness is preferred, as fully described elsewhere.[9]

**2.5. Gold Coating Procedure on Cell-Imprinted Substrates.** Prior to the stem cell seeding step and in vitro differentiation analysis, a thin layer of gold (Au) with an approximate thickness of 5−15 nm was deposited on the surface of the samples in a dc-sputtering unit (HIT, TECHNICS) at a base pressure of 10 mTorr. This procedure was designed to completely cover any remaining surface contamination. Additionally, this layer is exploited to enhance the conductivity of the elastomer or polystyrene samples, hence facilitating SEM imaging.

**2.6. Stem Cell Seeding on Cell-Imprinted Substrates.** The fabricated substrates were placed into the six-well plates. Then ADSCs (3 × $10^3$ cells/$cm^2$ in 100 μL of culture medium) were cultured onto the designed cell-imprinted substrates. After 1 day, 600 μL/$cm^2$ fresh DMEM/Ham's F12 (in a 3:1 ratio) and 10% (v/v) FBS medium was added to each substrate to completely cover it.

**2.7. Characterization of Cell-Imprinted Substrates by Scanning Electron Microscopy (SEM) and Atomic Force Microscopy (AFM).** The morphology of the various cell-imprinted substrates (PDMS) was observed with a Hitachi S4160 field emission (FE) scanning electron microscope (Hitachi Japan; apparatus working at 20 keV accelerating voltage). Formation of either fine structures or patterns within the cell-imprinted substrates prior to and after addition of cells was evaluated by AFM in both contact and noncontact modes. In this case, an NT-MDT AFM setup (Zelenograd, Moscow) with relative errors of the distance measurement of less than 1% in the *xy* plane and less than 5% in the *z* direction was used. The Nova PX software (version 3.1.0.0, NT-MDT) was utilized to analyze the AFM data obtained.

**2.8. Characterization of Stem Cells Cultured on Cell-Imprinted Substrates by Optical and Confocal Microscopy.** The morphological evaluation, cell growth, and specific protein expression detection of stem cells (freshly isolated ADSCs) which were grown on the 3D cell-imprinted silicone substrates were assessed by optical microscopy (Axioscope, Zeiss, Germany) and inverted confocal microscopy (Leica, TCS SP5, Germany). Prior to imaging, the cells were fixed in 4% formaldehyde for 15 min and permeabilized in a solution containing Triton X-100 in PBS for 5−10 min at room temperature. The cell nuclei were stained with propidium iodide (PI) (Invitrogen, United States). Control samples were cultured on 12 mm diameter circular glass coverslips. Stem cell differentiation was characterized using antihuman involucrin antibody, mouse antihuman pan-keratin antibody, and FITC-conjugated secondary antibody. Leica Application Suite Advanced Fluorescence (LAS AF) software (Leica Microsystems) was utilized to analyze the confocal microscope pictures.

**2.9. Gene Expression Profiling of Stem Cells Cultured on Cell-Imprinted Substrates.** *2.9.1. RNA Isolation and cDNA Synthesis.* Total RNA was extracted from the controls and cultured stem cells on substrates with the use of the TOP Animal Tissue and Cells RNA Purification Kit (TOPAZ, Iran) according to the manufacturer's instructions (directly applied to the cultured cells on the substrates). DNA was eliminated during RNA extraction utilizing DNase I according to the optional step in the RNA extraction kit. The concentration of cellular RNA was quantified by determining the maximum absorbance at a wavelength of 260 nm in a spectrophotometer (NanoDrop, Eppendorf, Germany). Finally, the complementary DNA (cDNA) was

synthesized with a Quanti Tect Reverse Transcription Kit (Qiagen, United States).

*2.9.2. Quantitative Real-Time Polymerase Chain Reaction (PCR).* The PCR assay was performed in a Step One instrument (Applied Biosystems, United States). As control samples, keratinocyte cells and ADSCs were cultured on plain substrate (PDMS without a cell-imprinted pattern) for 3 weeks after isolation. All reactions were carried out in duplicate, and each of them contained 20 $\mu$L of mixture solution including 10 $\mu$L of SYBR PCR Master Mix (ABI, United States), a 1 nM concentration of each primer, 3.5 $\mu$L of sterilized deionized water, and 4.5 $\mu$L of cDNA. Involucrin, keratin 10, and collagen type I were used as differentiation-specific markers, with GAPDH being used as an endogenous control for evaluation of differentiation. The primer pairs were designed using different software programs, namely, Beacon Designer v. 7.5, Gene Runner v. 3.05, and Primer Express v. 2.5, purchased from GeneAll (Seoul, Korea), and related sequences are shown in Table 1. The cycling conditions were as follows: one cycle of 95 °C for 10 min as the holding time and then 95 °C for 30 s (denaturation) and 60 °C for 1 min (annealing/extension), and the steps were repeated for 40 cycles. Amplification data were collected during the annealing/extension time. Melting curve analysis was performed as follows: reactions were heated to 95 °C for 15 s, followed by cooling to 60 °C and stepwise heating to 95 °C with a ramp rate of 0.3 °C. Finally, the comparative threshold cycle (CT) method (using the formula $2^{-\Delta\Delta(CT)}$) was used to analyze the data obtained.

**Table 1. Sequences of Primers Used in Real-Time PCR[a]**

| name of corresponding protein | | sequence |
|---|---|---|
| involucrin | Fw | 5′-TTCCTCCTCCAGTCAATACCCA-3′ |
| | Re | 5′-CTGTGGCTCCTTCTGCTGTTG-3′ |
| keratin 10 | Fw | 5′-TGAAGAAGAACCACGAGGAG-3′ |
| | Re | 5′-TGTTCAGCAAGTTGTTCATATTG-3′ |
| collagen type I | Fw | 5′-CGATGGCTGCACGAGTCA-3′ |
| | Re | 5′-GGTTCAGTTTGGGTTGCTTGTC-3′ |
| GAPDH | Fw | 5′-GAGTCCACTGGCGTCTTCA-3′ |
| | Re | 5′-TCTTGAGGCTGTTGTCATACTTC-3′ |

[a]Abbreviations: Fw, forward; Re, reverse.

**2.10. MD Simulation.** To investigate the effects of the nucleus geometry alteration on the chromatin conformation and ultimately gene expression, a simulation procedure was performed. This simulation was designed on the basis of the experimental results obtained from confocal microscopy (PI-stained nucleus).

In these simulations, chromatin fibers are modeled as coarse-grained bead−spring polymer chains. The chain energy ($U$) consists of several potentials: bonding energy ($U_{bond}$), bending energy ($U_{bend}$), and excluded volume potential ($U_{excl}$):[34,35]

$$U = U_{bond} + U_{bend} + U_{excl} = \sum_{i=1}^{N-1} \frac{1}{2} k_s (r_{i,i+1} - d_0)^2 + \sum_{i=1}^{N-2} \frac{1}{2} k_\theta (\theta_{i,i+1} - \theta_0)^2 + \sum_{i,j,i\neq j} 4\varepsilon \left[ \left( \frac{\sigma}{r_{i,j}} \right)^{12} - \left( \frac{\sigma}{r_{i,j}} \right)^{6} \right] \quad (1)$$

The stretching and bending stiffness are denoted by $k_s$ and $k_\theta$, respectively. The distance between the $i$th and $j$th beads is $r_{i,j}$, and the equilibrium distance between the neighboring beads is $d_0 = 2\sigma$, where $\sigma$ is the radius of each bead. The excluded volume potential was calculated by considering the repulsive part of the Lennard-Jones potential, and $\varepsilon$ denotes the depth of the well. The simulations were carried out in the LAMMPS program in the canonical ($NVT$) ensemble using the Nose−Hoover thermostat.[36] To entirely simulate the nucleus, another potential was introduced which applies spherical as well as ellipsoidal confinements to the chromatin fibers. This confining potential ($U_{conf}$), which resembles the nucleus membrane, was approximated by a repulsive Lennard-Jones wall. Additionally, to take into account the looping interactions, further simulations were carried out by subjecting the chromatin fibers to extra constraints. These constraints were approximated by additional harmonic restraints (i.e., same as the ones in the bonding potential) which connect random beads in a chain. In all simulations, 10 of the self-avoiding chains (each chain has 100 beads) as an initial configuration were generated. The system was equilibrated for $10^5$ MD time steps. Afterward, the chains underwent a three-stage confining procedure. First, a repulsive spherical wall was initially large enough to confine all chains. Its radius was shrunk slowly until the confined volume reached the desired value. The final volume of the spherical confinement was determined by the packing ratio (PR), which is defined as

$$PR = (\text{bead volume})/(\text{confined volume}) \quad (2)$$

The system was equilibrated for $10^6$ MD time steps. Then the confinement shape was changed from spherical to ellipsoidal with a constant volume. In the other step, the system was equilibrated for $10^6$ MD time steps, and the ellipsoidal confinement was reversibly changed into the initial spherical one. In all simulations, the parameter values (i.e., as currently identified from experiments) were utilized to approximate the mechanical properties of chromatin (Table 2).[34]

**Table 2. Parameter Values Used in the Coarse-Grained Model for Chromatin Simulations[34]**

| parameter | symbol | reduced units | SI units |
|---|---|---|---|
| thermal energy | $k_BT$ | 1.0 | $4.1 \times 10^{-21}$ J |
| bead mass | $m$ | 1.0 | $7.0 \times 10^{-21}$ kg |
| Lennard-Jones size parameter | $\sigma$ | 1.0 | 30 nm |
| Lennard-Jones energy parameter | $\varepsilon$ | 1.0 $k_BT$ | $4.1 \times 10^{-21}$ J |
| bead separation | $d_0$ | 1.0 $\sigma$ | 30 nm |
| contact distance | $d_c$ | 1.5 $\sigma$ | 45 nm |
| bond spring constant | $k_s$ | 500 $k_BT/\sigma^2$ | $2.3 \times 10^{-3}$ J m$^{-2}$ |
| persistence length | $L_p$ | 4.0 $\sigma$ | 120 nm |
| bending energy constant | $k_\theta$ | 4.0 $k_BT$/rad$^2$ | $1.7 \times 10^{-20}$ J rad$^{-2}$ |
| equilibrium angle | $\theta_0$ | $\pi$ | $\pi$ |

**2.11. Image Analysis Process.** To evaluate the changes in the morphology of the cultured ADSCs in different substrates, the image processing system CellProfiler 2.1.0 (revision 0c7fb94) was utilized.

**2.12. Statistical Analysis.** All data are expressed as the means ± SD of three separate experiments. Statistical significance was evaluated by one-way analysis of variance (ANOVA) and Student's $t$-test (SPSS software v. 17). A $P$ value of <0.01 was regarded as statistically significant.

## 3. RESULTS AND DISCUSSION

ADSCs were cultured on the keratinocyte-imprinted substrates as an in vitro replicate of the basal layer (deepest layer of the epidermis). The effects of these keratinocyte casts on the stem cell fate were evaluated by microscopical characterization (e.g., optical, confocal, SEM, and AFM) together with protein and gene expression analysis (real-time PCR). A schematic of the experimental setup and exact mechanism of this study is shown in Figure 1.

**3.1. Fabrication and Imprinting Procedure of Keratinocyte Membrane Patterns on a Silicone Substrate and Their Characterization.** The 3D cell-imprinted PDMS substrates were prepared using our surface imprinting method. PDMS is recognized as a promising material for accurate cell imprinting, as during the molding and curing process it slowly flows and adjusts to the required topography. In addition, PDMS's innate characteristics such as soft consistency, transparency, and biocompatibility are also advantageous.

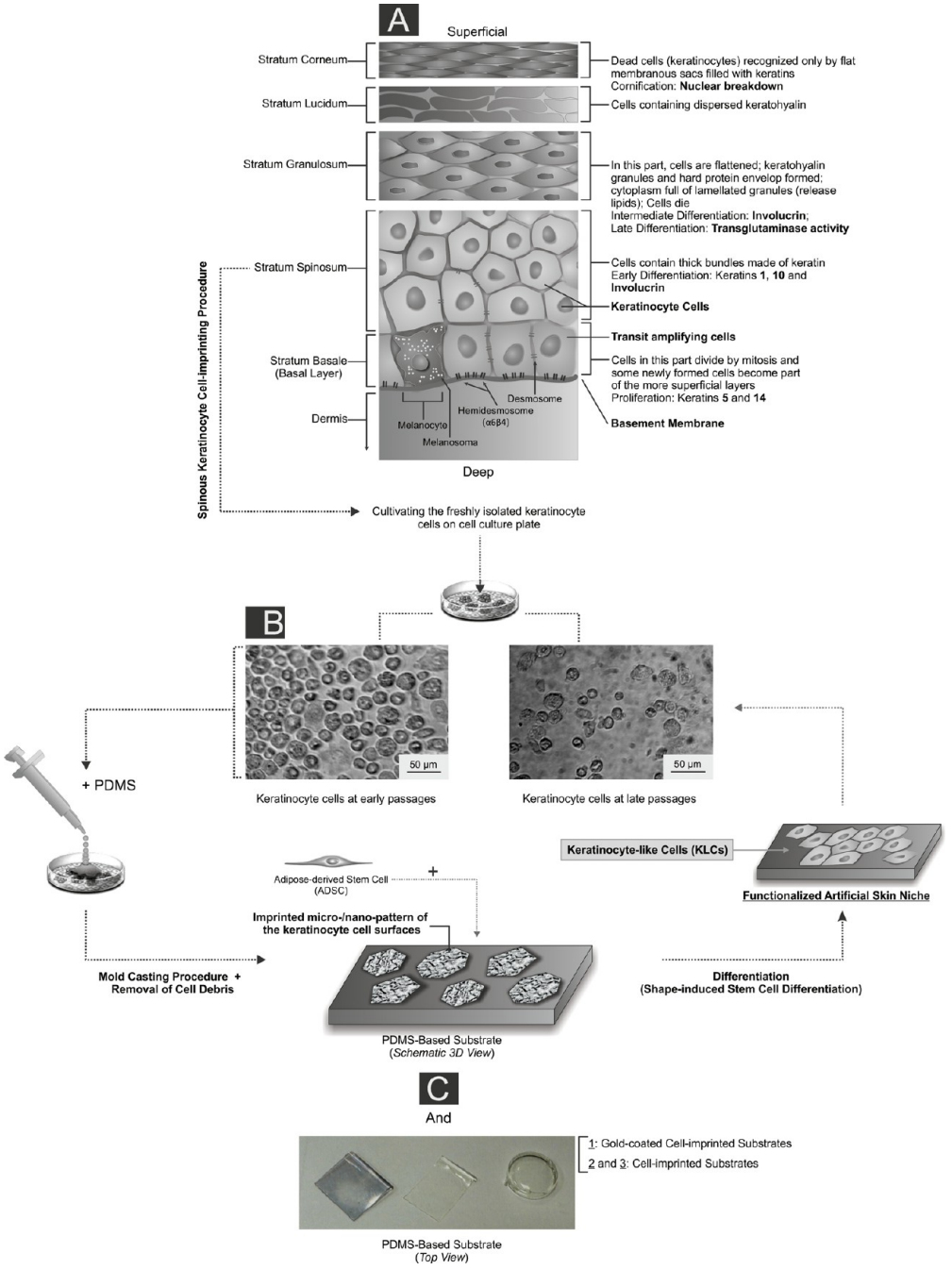


**Figure 1.** Detailed architecture of the basal-to-spinous layer transition together with an illustration of the experimental setup and artificial skin niche study steps. (A) The program of epidermal differentiation is illustrated, exposing the basement membrane at the base, the proliferative basal layer, and the four differentiation stages: stratum spinosum layer, stratum granulosum layer, stratum lucidum layer, and outermost stratum corneum. The key molecular markers which are shown in this schematic are described in detail in the paper. The proliferative basal cells, as a multipotent progenitor of the epidermis layer, adhere to an underlying basement membrane (separating the dermis from the epidermis) and can differentiate into the spinous cells in the suprabasal layer. Quiescent human epidermal stem cells and their transient amplifying cell progeny give rise to a column of differentiated keratinocytes in diverse layers as depicted. The transit-amplifying cells constantly produce progeny which move upward as they terminally differentiate and are ultimately lost from the skin surface (superficial). (B) The cultivated keratinocyte cells on different well plates at different passage levels are shown. (C) To fabricate the PDMS-based substrate which mimics the natural stratum spinosum layer's function, the keratinocyte cells were grown on a cell culture plate and their complete morphologies at different stages were transferred to a silicone replica by a mold casting procedure. After the removal of damaged cells and cell debris from the substrates, a negative PDMS-based replica (i.e., noncoated and gold-coated heterostructure substrates with varied thicknesses) with an imprinted pattern of the cell surfaces was achieved. This unique structure was utilized as an efficient platform to manipulate the stem cells to achieve production of the keratinocyte-like cells.

For cell imprinting, fresh keratinocyte cells were cultivated on tissue culture polystyrene plates over 2 weeks. They were fixed with glutaraldehyde before PDMS was poured over them to maintain the cellular shape during the imprinting processes. It is also worth noting that the keratinocyte cells at early passages were easily identified as homogeneous monolayers of small (20−30 $\mu$m in diameter) polygonal cells, whereas they became irregular in size and shape at later passages (40−50 $\mu$m in diameter)

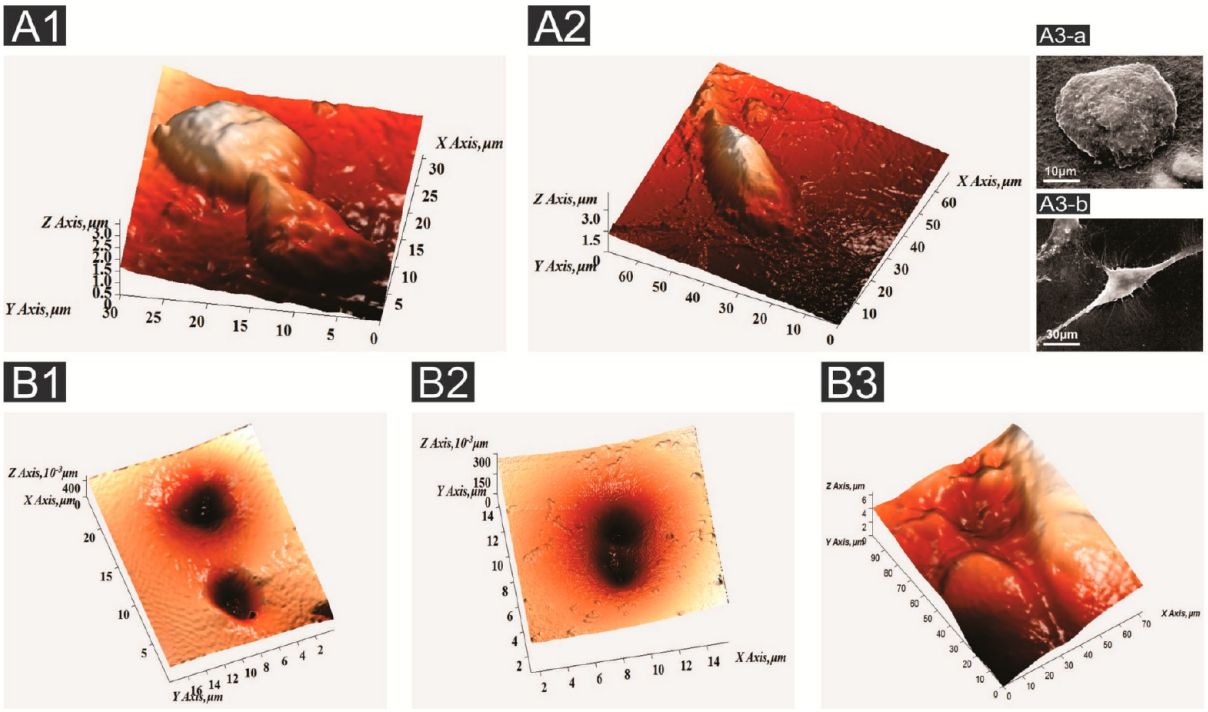


**Figure 2.** AFM images in contact mode topography of the studied keratinocyte cells which were cultivated on the 24-well plates in the 3D model (A1) together with the SEM result (A3-a). The 3D image in (A2) shows a cultured stem cell on the 24-well plates together with the SEM result (A3-b). The 3D AFM images in contact mode show the topography of the silicone-based substrates with keratinocyte-cell-imprinted patterns (fingerprints) prepared by mold casting on a collagen-coated well plate (polystyrene plate) (B1) and that of keratinocytes which were cocultured with growth-arrested 3T3 MEFs (B2). The 3D AFM image in contact mode shows the topography of the silicone-based substrates with stem-cell-imprinted patterns (fingerprints) prepared by mold casting on a collagen-coated well plate (polystyrene plate) (B3).

(Figure 1B). In light of this, cell-imprinted substrates were prepared from early passage keratinocyte cells.

**3.2. Analysis of Patterned Cells (HKs) in Various Culture Conditions.** To investigate the optimal keratinocyte layer for cell imprinting, three different cell culture conditions were employed to culture keratinocyte cells: (i) PDMS was added to cultivated keratinocytes on 24-well plates which were coated with collagen type I solution. Generally, ECM components such as collagen and fibronectin are employed to coat the well plates or coverslips to enhance cell attachment. In this case, collagen-promoted cell attachment was observed. (ii) PDMS was added to the keratinocyte−3T3 mouse embryonic fibroblast cocultured cells. Experiments where keratinocytes have been cocultured with fibroblasts have demonstrated stimulation of the keratinocyte phenotype.[37] Here, keratinocyte proliferation was stimulated by 3T3 cells in the coculture platform (the cells reached 70% confluence and were ready for passage within 10 days).[38] (iii) PDMS was added to the keratinocytes which were cultured on 96-well plates without any collagen or feeder layer.

Prior to analysis of the keratinocyte cell patterns, the optimal substrates were preselected by optical microscopy (Figure 1C). For the keratinocyte cells which were cultured on collagen type I, AFM in contact mode revealed a typical semispherically shaped cell topography in 3D and 2D models (Figure 2A1; Figure S1, Supporting Information). The average heights of the keratinocyte cells are demonstrated in Figure S8 (Supporting Information). SEM images of the keratinocytes revealed good cell attachment on the collagen-coated surface. We note that stem cells could also attach well to the collagen-coated surface (Figure 2A3-b; Figure S3-b, Supporting Information) and the stem cells and keratinocytes had distinct morphologies (Figures S8 and S9). It is noteworthy at this point that each specific cell type in the human body has its specific size and shape, which contribute to a specific function; the cell function would change if the cell lost its inherent shape.[39,40] We thus selected this surface as our optimal platform for our printing procedure (Figures 2A3-a and S3-a).

The layer thicknesses of the imprinted PDMS substrates, after peeling, varied in the range of 1−2 mm. To completely remove the attached cells, debris, and chemical/biomolecular residues, numerous washing steps were performed with 1 M NaOH solution. Additionally, it was hypothesized that the cell membrane fragments or molecular residues may play a role as a chemical cue which can modulate the stem cell fate.[20,26,41] Thus, the substrates were autoclaved at 120 °C to deactivate the remaining biomolecules at the surface of the imprinted substrates. In addition, prior to cell culturing, a thin layer of gold (Au) with an approximate thickness of 5−15 nm was deposited on the surface of the obtained substrates by dc-sputtering to completely cover the possibly remaining cell membrane fragments. In our previous work it was shown that the morphology of the cavities on the PDMS surface is preserved.[9] Furthermore, it has been demonstrated that the thin deposited gold nanolayer did not have a significant effect on the stem cell fate (i.e., it had no effect on the gene expression results).[9]

**3.3. Analysis of the Cell-Imprinted PDMS Surfaces.** To probe the quality of the cell-imprinted surface, such as topography and fidelity, the cell-imprinted replicas were characterized by AFM and SEM. The AFM evaluation of the substrates showed high fidelity, with the cell morphology being faithfully reproduced (see Figure 2B1−B3). It was noted that the imprinting

from the collagen-coated surfaces had better resolved features compared to the other strategies (Figure 2B1,B2; Figures S5, S6, S10, and S11, Supporting Information). In addition, with the coculture system, there were some particles appearing on the substrate surfaces which might have an influence on the differentiation process (Figures 2B2 and S5). Interestingly, the membrane features of the keratinocyte cells were imprinted on the substrates (Figure 3C1−C3). For comparison, we also made

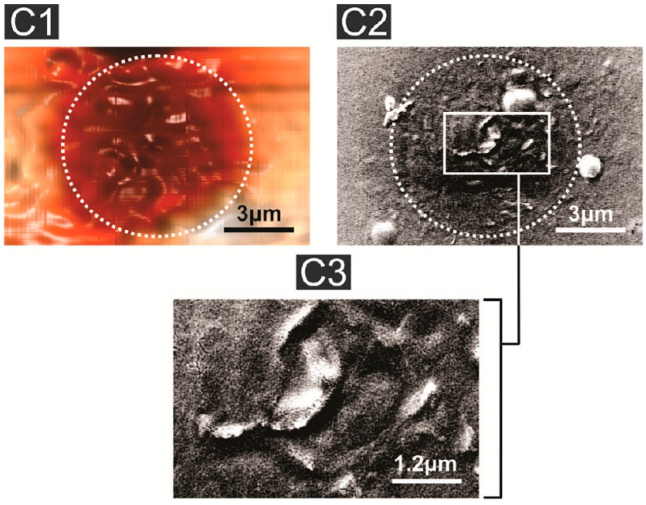


**Figure 3.** (C1) High-resolution AFM scan (512 × 512 pixel resolution) of a single groove with distinct patterns which was in good agreement with the SEM results (C2, C3).

imprints using stem cells as substrates. The stem cells formed distinct semispindle-shaped casts with numerous branches (Figure 2B3; Figures S6 and S7, Supporting Information), providing close fidelity to their original form (Figure 2A2). In fact, the size and architecture of such depressions were completely different with respect to those obtained from keratinocyte cell imprinting. Note that we have previously measured the roughness of our plane control materials to be negligible.[9]

**3.4. ADSC Fate Dictated Exclusively by Cell-Imprinted Patterns: Hypothesis of the Functionalized Artificial Skin Niche.** ADSCs were cultivated on gold-coated cell-imprinted PDMS substrates (Figure 1C). Interestingly, after 3 days of culture, the attached ADSCs on the fabricated keratinocyte casts imitated the normal keratinocyte irregular polygonal shape (Figure 4D1; Figure S13, Supporting Information). SEM and AFM results showed that while some stem cells which did not comply with the negative patterned surfaces maintained their natural shape (elongated spindle form) (Figure 4D2), many did undergo a shape/topology-induced morphology change on the substrates (Figure 4D3).[42] The observed morphology of the ADSCs grown on the keratinocyte imprints was noticeably different from that of stem cells cultured on stem-cell-imprinted substrates (Figure 4D1,D4; Figure S14, Supporting Information). To have a better understanding of the morphological changes of the cultured stem cells on different substrates, an image analysis process was performed; the results confirmed considerable stem cell expansion during culturing on stem-cell-imprinted substrates (Figures S15 and S16, Supporting Information).

Numerous studies have previously indicated that stem cell fate is regulated by a combination of intrinsic (e.g., specific transcription factors) and extrinsic mechanisms which are provided by the local microenvironment (i.e., niche).[4,20] These specific or nonspecific interactions direct stem cells to sense the different mechanical cues (i.e., mechanotransduction process).[43] Such mechanotransductive changes can be derived intracellularly from rearrangement of adhesions and the cytoskeleton on the basis of changes in the ECM or synthetic substrates causing changes in cell contractility.[44,45] Such mechanotransductive events have now been studied at the single-cell level using micropatterned substrates, and it has been shown this can direct the cell fate.[46,47]

In this respect, to analyze the phenotypical effects of mechanoshape-driven differentiation for keratinocyte-cell-imprinted islands, the PCR methodology was employed. In this study, for the 2 week culture of ADSCs on the substrates, gene expression levels of involucrin, collagen type I, and keratin 10 for each sample (i.e., stem/keratinocyte-cell-imprinted substrates) were compared with those of the controls (i.e., cell culture well plates) (Figure 5A). The results revealed that the expression of keratinocyte-specific markers (i.e., keratin 10 (K10, cytokeratin 10) and involucrin (IVL)) by ADSCs after culture on keratinocyte-cell-imprinted patterns was significantly higher than that after culture on stem-cell-imprinted patterns (Figure 5B). As shown in Figure 1A, K10 is a key early marker for keratinocyte differentiation of the stratum spinosum layer and involucrin is a specific marker for an early stage in the pathway of terminal epidermal proliferation and differentiation.[48,49] On the basis of the PCR data, the ADSCs cultured on the silicone substrates with the keratinocyte-imprinted patterns expressed the keratinocyte-specific gene markers K10 and IVL, but those that were cultured on the silicone substrates with imprinted patterns of the elongated spindle form stem cells did not express the keratinocyte markers and exhibited/maintained their native gene expression profile. These results support our hypothesis, on a molecular level, that topographical patterns can induce stem cell differentiation to a targeted lineage. According to previous research, geometrically optimized surfaces of tissue culture plastic can promote the self-renewal of embryonic stem cells and induced pluripotent stem cells (iPSCs) in the absence of feeder cells.[24,50] Furthermore, to evaluate the feasibility of ADSC differentiation capacity into keratinocytes, cytokeratin and IVL antibodies were utilized, since they are specific markers for basal keratinocytes. In this context, ADSCs were seeded on different substrates and immunostained with an antihuman IVL antibody and antihuman pan-keratin antibody. Keratinocytes on six-well plates and ADSCs on stem-cell-imprinted substrates were used as positive and negative controls, respectively (Figure 5C−E). As shown in Figure 5C,D, as early as 14 days on the keratinocyte-cell-imprinted substrates, we start seeing positive staining for cytokeratin (green) and IVL (green). Besides the results obtained by AFM and SEM, the stem cell 3D shape mimicking phenomena could also be distinguished by confocal imaging (i.e., the white outline shows the altered cell shape in the keratinocyte-cell-imprinted substrates) (Figure 5C,D).

Our results indicated not only morphological changes of the ADSCs (Figure 4), but also targeted genotypic changes in the cells (Figure 5), demonstrating the capability of the keratinocyte-cell-imprinted substrates to differentiate the ADSCs into KLCs to create a stratified epidermis-like structure. Although it has been recognized for several years that the ECM structure is a key component of the stem cell niche, our results at single-cell resolution have provided novel information about the underlying mechanism by which the single-cell-imprinted pattern (cell membrane topography) regulates stem cell behavior and function.[51,52]

This new paradigm of cell morphology replicas inducing defined phenotypes has really developed seminal work on form

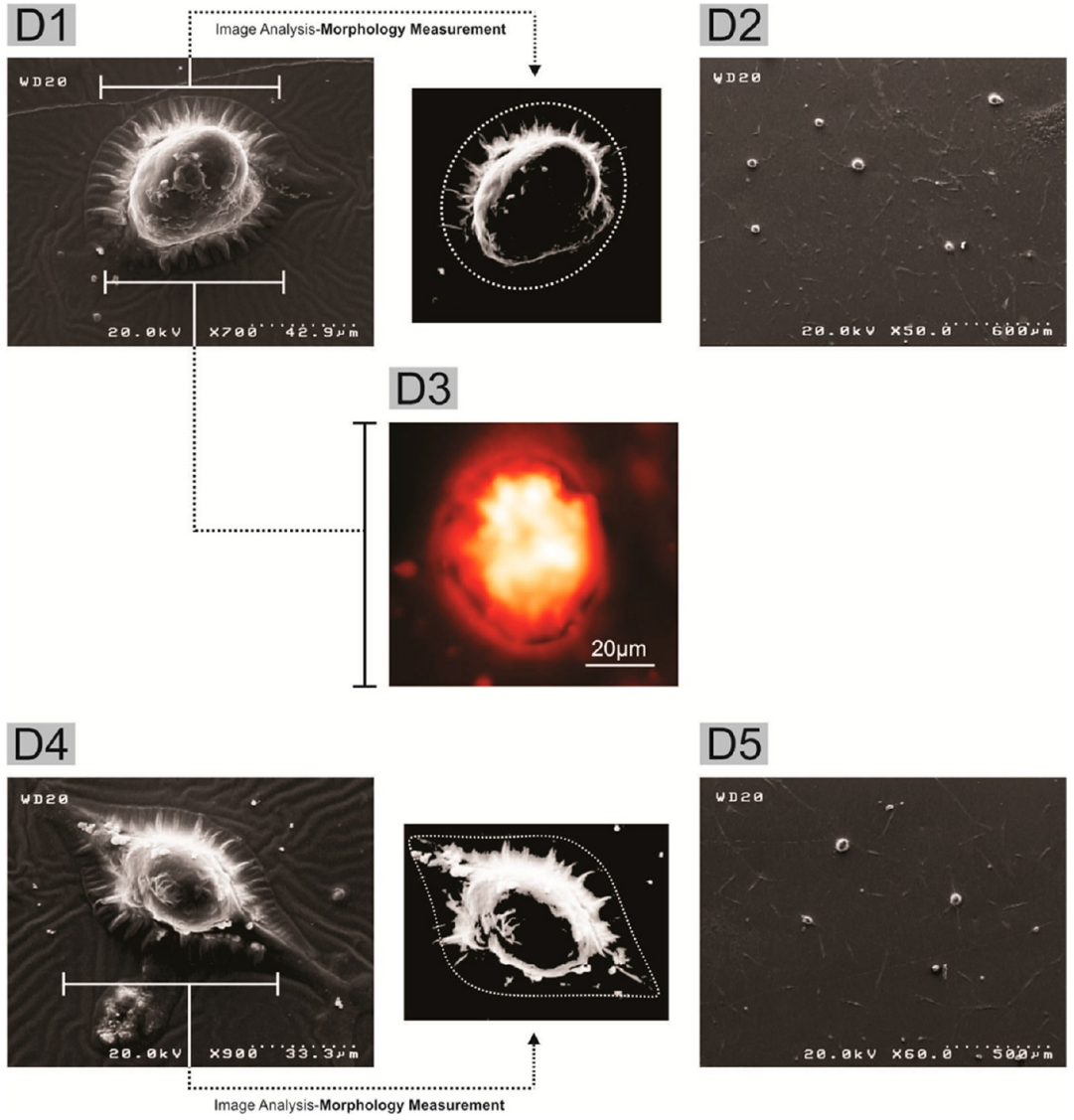


**Figure 4.** Morphological alterations of mesenchymal ADSCs which were grown on keratinocyte-cell-imprinted silicone substrates (D1, D2) and stem-cell-imprinted substrates (D4, D5) at different magnifications. The AFM image shows the detailed morphology obtained on keratinocyte-cell-imprinted replicas for ADSCs (D3). Image analysis illustrates the changes in the morphology of the stem cells (i.e., ellipticity/sphericity) on different imprinted substrates.

and function. Our approach takes Ingber's ideas on tissue function following form[53] through the reductionist approaches of cell confinement driving differentiation depending on the size at which the cells were held[47,54] to an ultimate conclusion of molding a stem cell to the morphology that you desire and achieving the desired phenotype.

**3.5. Computational Observation of Nucleus Geometry Alteration.** On the basis of the observation that the nucleus shape changes when the cell's fate is altered, we carried out simulations to investigate the effect of nucleus geometries on the contacts between chromatin fibers and their arrangements.

After noting shape-induced differentiation, we decided to focus on the nucleus. The nucleus is connected to the cytoskeleton through LINC (linkers of the nucleoskeleton and cytoskeleton) complexes, and it is likely that nuclear shape changes are driven by cell shape changes. Thus, it can be considered that gene expression profiling could be altered by physicochemical cues on the nanoscale from the local microenvironment and this could contribute to phenotype determination.[40,55] Numerous of canonical signaling pathways are activated in response to the cellular matrix and geometric cues converging on diverse transcription factors (e.g., NF$\kappa$B).[55,56] However, it has also been demonstrated that the physical transmission of such stresses through cytoplasmic−nuclear connections can potentially remodel the chromatin structure.[55] It is likely that in our experiments the changes in cell morphology and alterations in intracellular cytoskeletal tension will not just affect the biochemistry but will also alter the nucleus morphology. To shed more light on this claim, we performed computational modeling to probe the effects of the confining geometry on the chain arrangement of chromatin fibers in the nucleus. In the simulation, chromatin fibers were modeled as flexible elastic polymer chains. During the experiment, the simulated polymer chains were represented as chromosome territories (CTs) (i.e., the genome itself in the cell nucleus is organized into loops and is partitioned into functional chromosome territories).[57] The experimental results showed that the geometry and shape of the cultivated stem cell nucleus were altered from an ellipsoidal shape to a spherical one during the differentiation process on the cell-imprinted substrates

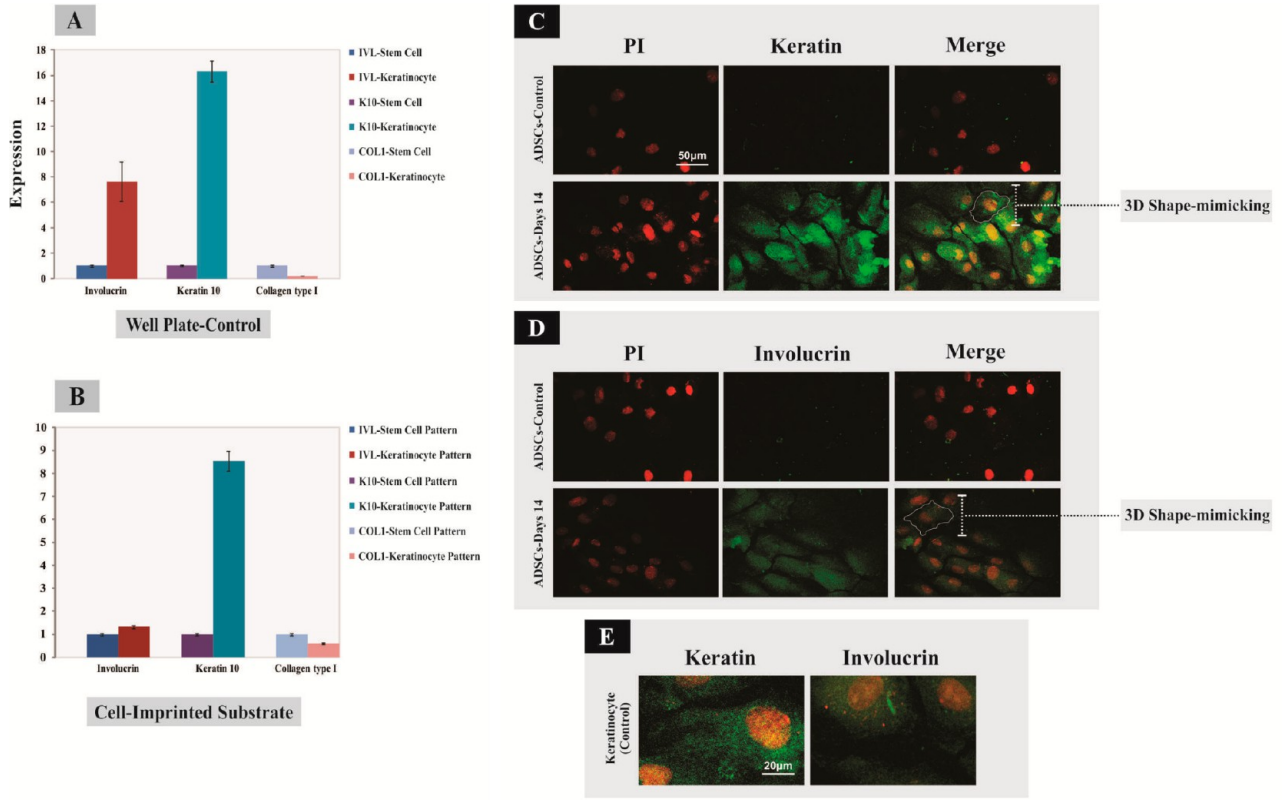


**Figure 5.** Quantitative real-time PCR analysis: Gene expression profile of freshly isolated keratinocytes and ADSCs which were grown on standard cell culture well plates as control substrates (A), together with the cultivated ADSC gene expression level for the collagen type I (COL1) substrates and IVL and K10 genes on the stem-cell- and keratinocyte-imprinted substrates (B). Immunocytochemistry confirmed the expression of cytokeratin (green) (C) and IVL (green) (D) in the cultured ADSCs on the keratinocyte-imprinted substrates after 14 days of cell culture. (E) Keratinocytes which were grown on standard cell culture well plates as a control for the antihuman IVL antibody and mouse antihuman pan-keratin antibody. A very low autofluorescence background was detected for the used substrates.

(Figure 6A). In this procedure, the cell shape analysis, performed using confocal microscopy, was repeated for six samples—for both cell-imprinted and planar substrates. Afterward, the utilized substrates were divided to five equal parts, and for each part a total of 50−100 ADSCs were selected and assessed.

The confining sequence (i.e., primary spherical to ellipsoidal and then to secondary spherical) of the chains is illustrated in Figure 6B. Since in our simulations the initial conformation of the chromatin fibers is required to be energetically relaxed, no confinement is imposed on the initial conditions. Then a sufficiently large spherical confinement was used to envelop all the simulated fibers and reduce their volume to achieve the desired packing ratio. Hence, the ultimate geometry of the confinement is shown S1 in Figure 6B. Afterward, the spherical confinement (S1) changed into an ellipsoidal one (S2) to resemble the initial ellipsoid-shaped nucleus of undifferentiated stem cells. In the next step, the geometry of the ellipsoidal nucleus was gradually altered into a spherical shape (S3), which was experimentally observed when the stem cells were cultured on the keratinocyte-cell-imprinted substrate (differentiated cells). On the basis of previous reports,[58,59] specialized cells experienced dramatic changes in nuclear shape (the cell nucleus typically maintains spheroidal or ellipsoid morphologies) during the differentiation and maturation process. It should be noted that, due to the reduced cytoplasmic to nuclear ratio in stem cells, the chromosomes are highly plastic in these cells.[60] Differentiated cells from diverse tissues may comprise distinctive cell-type-specific positional ordering of chromosomes.[61]

Additionally, the packing procedure of the coarse-grained bead−spring polymer chains and the nucleus geometry alteration are shown in animations 1−4 of the Supporting Information. To have better understanding of the 3D spatial organization of the chromatin fibers, the contact probability method was used. In this methodology, a matrix was defined over all pairs of the chromatin beads, such that the arrays of the matrix exhibited the contact probabilities between two pairs of fibers. These probability values varied from 0 (no contact between the beads) to 1 (the selected beads are in contact) (the details of the contact probability calculation can be found in the Supporting Information).

In all procedures performed, the volume of confinement, and accordingly the packing ratio, was maintained as a constant to eliminate the effects of volume change in contact probability matrices. In each confining stage, two contact probability matrices were calculated:[62] (i) One of the matrices, which was called a bead-contact probability (BCP) matrix, was utilized to describe the contact probability among the beads. (ii) Second, a chain-contact probability (CCP) matrix was used to explain the contact probability among the chains (the calculation procedure of the BCP and CCP matrices can be found in the Supporting Information) (Figure S17). It is worth noting that Figure S17 illustrates the connectivity map among the beads (BCP) and chains (CCP) for the simulated nucleus.

To quantitatively differentiate the 3D organization of the chromatin fibers between two confinement stages, i and j, a dissimilarity distance ($D_d^{i-j}$) was introduced (the calculation procedure

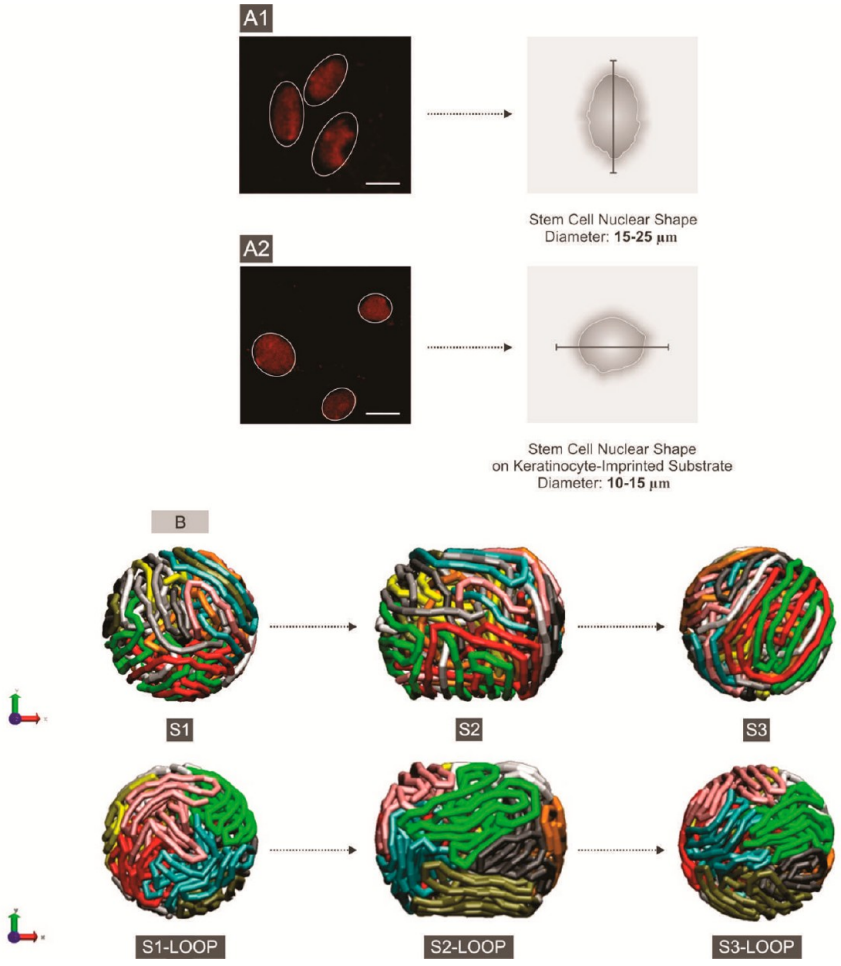


**Figure 6.** (A) Confocal microscopy images of the nucleus for the cultivated stem cells which were stained with PI (red) on the control well plates (A1) and cell-imprinted substrates (A2) together with the illustrated schematic of the nucleus shape and diameter (bars = 30 $\mu$m). (B) Snapshots of the chromatin fibers for different shapes of the confinements. The first and second rows show the simulated systems in which the free and looped chains are confined, respectively. The three stages of the confinements are named S1, S2, and S3 and represent the primary spherical and ellipsoidal and secondary spherical confinements in turn. The packing ratio during the process of the confinement change remained constant. The graphical representations are carried out with VMD software.[70]

is included in the Supporting Information). The obtained dissimilarity distances between three confining stages are shown in Figure 7. The results indicate the strong influence of the geometry of the confinement on the chain organization. Interestingly, in this simulation, the dissimilarity distance between the primary and secondary spherical confinements ($\|S_1 - S_3\|$) indicated that the conformational organizations of the simulated chromatin in the differentiated cells were not reversible. It is worth noting that when the chromatin fibers experienced higher packing ratios due to less free space being available (i.e., enough space to change the conformations of the chromatin) in the presence of thermal fluctuations, the dissimilarity distances in all three stages became smaller.

In addition, the corresponding contact maps for both cases (spherical and ellipsoidal) were calculated to investigate the alteration effects of the confining geometries on the arrangement of the chromatin fibers. On the basis of the simulation modeling results, the dissimilarity distances (i.e., calculated by the Euclidian distance between the contact maps) were influenced by the geometry alteration, becoming larger compared to the distance caused by thermal fluctuations. Eventually, by having confined chromatin fibers, the nucleus can change its spherical geometry into an ellipsoidal one while preserving its volume. This can introduce a measure of the dissimilarity distance by the contact probability matrix system, which could statistically analyze the adjacency within chromatin fibers in our modeling. Our results revealed that while the adjacency matrix between the chains is almost stable for a fixed geometry of the nucleus wall, the local organization of chromatin fibers inside the nucleus is affected by deformation of the confining nucleus, and finally, the performed simulations show that the change in adjacency is not reversible.

From the experimental point of view, numerous microenvironmental cues can regulate the stem cell fate to the different lineages by the cell shape and cytoskeletal tension (i.e., RhoA signaling).[10,20,54] In this regard, cytoskeletal filaments, as highly cross-linked gel-like structures, may act as cables to transmit environmental stresses across a distance, providing the cytoplasmic inhomogeneity required to transmit force.[63] Chromatin-remodeling enzymes (e.g., histone acetylase transferases) may alter the chromatin structure.[64] Furthermore, alteration of the lamin concentration, especially A/C lamins, has been suggested as a main modulator of nuclear mechanics.[65] For instance, stem cells express no A/C lamins in the lamina. Lamin A/C then contributes to the lamina as stem cells differentiate,[60] altering the nuclear shape and stiffness.[60,66] Additionally, several experimental and computational studies have demonstrated the diverse effects of intra- and

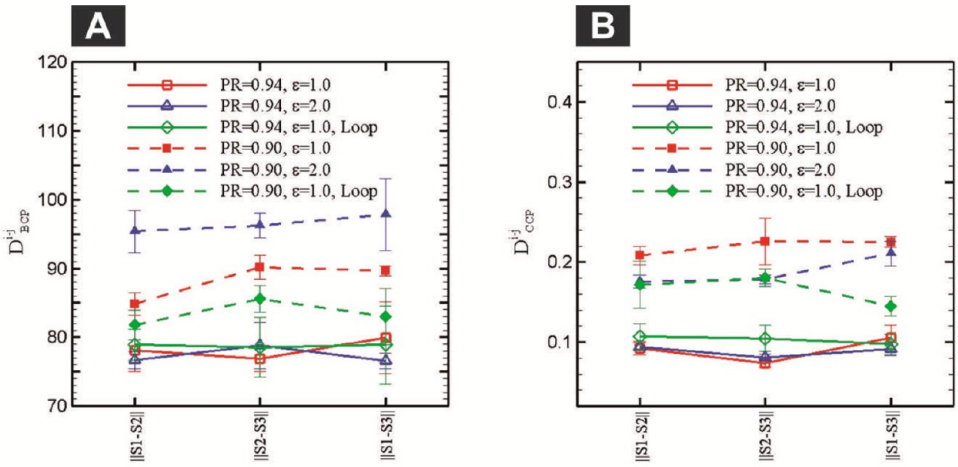


**Figure 7.** Dissimilarity distance between different types of confinements calculated over the BCP (A) and CCP (B) matrices together with an illustration of different repulsive strengths of the excluded-volume potential ($\epsilon$) as well as different PRs.

extracellular forces on the nuclear shape, suggesting changes in cell signaling and gene transcription.[62,67−69]

Therefore, on the basis of the evidence provided by the proposed computational model, the experimentally observed phenomenon of nucleus shape deformation on the cell-imprinted substrates could be at least partly responsible for regulating target genes in vitro. This hypothesis needs further investigation.

## 4. CONCLUSIONS

In this study, we hypothesized that induction of the mature keratinocyte shape to stem cells could result in differentiation of stem cells to KLCs. We observed that the ADSCs adopted keratinocyte-like morphologies and expressed keratinocyte marker genes and proteins. Our data further imply a role of direct mechanotransduction to the nucleus as well as biochemical mechanotransduction. In our molecular dynamics simulations, chromatin fibers were modeled as coarse-grained bead−spring polymer chains and the nucleus geometry was simulated by a repulsive wall. In our modeling system, a measure of dissimilarity distance was introduced by the contact probability matrix to statistically analyze the adjacency within chromatin fibers. The simulations showed that the change in adjacency was not reversible, and the obtained results supported the hypothesis in which mechanical deformation may induce transduction by affecting the chromatin fiber arrangement inside the stem cell nucleus. Our work proves conclusively that stem cell function does follow form; make a stem cell look like you want it to act like and it does so.

## ■ ASSOCIATED CONTENT

### Supporting Information

Detailed microscopy data (i.e., AFM, SEM, optical), detailed results of the image analysis process and computational observation of nucleus geometry alteration, and animation files (MPG) for the formation of packing of the free and looped chains in the various PRs together with the deformation sequence of the free and looped chains in the three stages of confinement. This material is available free of charge via the Internet at http://pubs.acs.org/.

## ■ AUTHOR INFORMATION

### Corresponding Author

*(S.B.) E-mail: sh_bonakdar@pasteur.ac.ir

*(M.M.) Phone: +98-9125791557. Fax: +98-2122568051. E-mail: mahmoudi-m@tums.ac.ir.

### Present Address

□Division of Pediatric Cardiology, Department of Pediatrics, Stanford University School of Medicine, Stanford, California 94305-5101, United States

### Notes

The authors declare no competing financial interest.

## ■ REFERENCES

(1) Takahashi, K.; Yamanaka, S. Induction of Pluripotent Stem Cells from Mouse Embryonic and Adult Fibroblast Cultures by Defined Factors. *Cell* **2006**, *126*, 663−676.

(2) Pardal, R.; Clarke, M. F.; Morrison, S. J. Applying the Principles of Stem-Cell Biology to Cancer. *Nat. Rev. Cancer* **2003**, *3*, 895−902.

(3) Czyz, J.; Wobus, A. M. Embryonic Stem Cell Differentiation: The Role of Extracellular Factors. *Differentiation* **2001**, *68*, 167−174.

(4) Guilak, F.; Cohen, D. M.; Estes, B. T.; Gimble, J. M.; Liedtke, W.; Chen, C. S. Control of Stem Cell Fate by Physical Interactions with the Extracellular Matrix. *Cell Stem Cell* **2009**, *5*, 17−26.

(5) Reilly, G. C.; Engler, A. J. Intrinsic Extracellular Matrix Properties Regulate Stem Cell Differentiation. *J. Biomech.* **2010**, *43*, 55−62.

(6) Scadden, D. T. The Stem-Cell Niche as an Entity of Action. *Nature* **2006**, *441*, 1075−1079.

(7) Daley, W. P.; Peters, S. B.; Larsen, M. Extracellular Matrix Dynamics in Development and Regenerative Medicine. *J. Cell Sci.* **2008**, *121*, 255−264.

(8) Dalby, M. J.; Gadegaard, N.; Tare, R.; Andar, A.; Riehle, M. O.; Herzyk, P.; Wilkinson, C. D.; Oreffo, R. O. The Control of Human Mesenchymal Cell Differentiation Using Nanoscale Symmetry and Disorder. *Nat. Mater.* **2007**, *6*, 997−1003.

(9) Mahmoudi, M.; Bonakdar, S.; Shokrgozar, M. A.; Aghaverdi, H.; Hartmann, R.; Pick, A.; Witte, G.; Parak, W. J. Cell-Imprinted Substrates Direct the Fate of Stem Cells. *ACS Nano* **2013**, *7*, 8379−8384.

(10) Engler, A. J.; Sen, S.; Sweeney, H. L.; Discher, D. E. Matrix Elasticity Directs Stem Cell Lineage Specification. *Cell* **2006**, *126*, 677−689.

(11) Chen, W.; Villa-Diaz, L. G.; Sun, Y.; Weng, S.; Kim, J. K.; Lam, R. H.; Han, L.; Fan, R.; Krebsbach, P. H.; Fu, J. Nanotopography Influences Adhesion, Spreading, and Self-Renewal of Human Embryonic Stem Cells. *ACS Nano* **2012**, *6*, 4094−4103.

(12) Fisher, O. Z.; Khademhosseini, A.; Langer, R.; Peppas, N. A. Bioinspired Materials for Controlling Stem Cell Fate. *Acc. Chem. Res.* **2009**, *43*, 419−428.

(13) Vogel, V.; Sheetz, M. Local Force and Geometry Sensing Regulate Cell Functions. *Nat. Rev. Mol. Cell Biol.* **2006**, *7*, 265−275.

(14) McNamara, L. E.; Burchmore, R.; Riehle, M. O.; Herzyk, P.; Biggs, M. J.; Wilkinson, C. D.; Curtis, A. S.; Dalby, M. J. The Role of Microtopography in Cellular Mechanotransduction. *Biomaterials* **2012**, *33*, 2835−2847.
(15) Tsimbouri, P. M.; Murawski, K.; Hamilton, G.; Herzyk, P.; Oreffo, R. O.; Gadegaard, N.; Dalby, M. J. A Genomics Approach in Determining Nanotopographical Effects on MSC Phenotype. *Biomaterials* **2013**, *34*, 2177−2184.
(16) Wan, L. Q.; Kang, S. M.; Eng, G.; Grayson, W. L.; Lu, X. L.; Huo, B.; Gimble, J.; Guo, X. E.; Mow, V. C.; Vunjak-Novakovic, G. Geometric Control of Human Stem Cell Morphology and Differentiation. *Integr. Biol.* **2010**, *2*, 346−353.
(17) Tang, J.; Peng, R.; Ding, J. The Regulation of Stem Cell Differentiation by Cell-Cell Contact on Micropatterned Material Surfaces. *Biomaterials* **2010**, *31*, 2470−2476.
(18) Yim, E. K.; Pang, S. W.; Leong, K. W. Synthetic Nanostructures Inducing Differentiation of Human Mesenchymal Stem Cells into Neuronal Lineage. *Exp. Cell Res.* **2007**, *313*, 1820−1829.
(19) Holle, A. W.; Tang, X.; Vijayraghavan, D.; Vincent, L. G.; Fuhrmann, A.; Choi, Y. S.; Álamo, J. C.; Engler, A. J. In Situ Mechanotransduction via Vinculin Regulates Stem Cell Differentiation. *Stem Cells* **2013**, *31*, 2467−2477.
(20) Watt, F. M.; Huck, W. T. Role of the Extracellular Matrix in Regulating Stem Cell Fate. *Nat. Rev. Mol. Cell Biol.* **2013**, *14*, 467−473.
(21) Nikukar, H.; Reid, S.; Tsimbouri, P. M.; Riehle, M. O.; Curtis, A. S.; Dalby, M. J. Osteogenesis of Mesenchymal Stem Cells by Nanoscale Mechanotransduction. *ACS Nano* **2013**, *7*, 2758−2767.
(22) McMurray, R. J.; Gadegaard, N.; Tsimbouri, P. M.; Burgess, K. V.; McNamara, L. E.; Tare, R.; Murawski, K.; Kingham, E.; Oreffo, R. O.; Dalby, M. J. Nanoscale Surfaces for the Long-Term Maintenance of Mesenchymal Stem Cell Phenotype and Multipotency. *Nat. Mater.* **2011**, *10*, 637−644.
(23) Tsimbouri, P.; Gadegaard, N.; Burgess, K.; White, K.; Reynolds, P.; Herzyk, P.; Oreffo, R.; Dalby, M. J. Nanotopographical Effects on Mesenchymal Stem Cell Morphology and Phenotype. *J. Cell. Biochem.* **2014**, *115*, 380−390.
(24) Mei, Y.; Saha, K.; Bogatyrev, S. R.; Yang, J.; Hook, A. L.; Kalcioglu, Z. I.; Cho, S.-W.; Mitalipova, M.; Pyzocha, N.; Rojas, F. Combinatorial Development of Biomaterials for Clonal Growth of Human Pluripotent Stem Cells. *Nat. Mater.* **2010**, *9*, 768−778.
(25) Dalby, M. J.; Gadegaard, N.; Oreffo, R. O. Harnessing Nanotopography and Integrin-Matrix Interactions to Influence Stem Cell Fate. *Nat. Mater.* **2014**, *13*, 558−569.
(26) Lutolf, M. P.; Blau, H. M. Artificial Stem Cell Niches. *Adv. Mater.* **2009**, *21*, 3255−3268.
(27) Lutolf, M. P.; Gilbert, P. M.; Blau, H. M. Designing Materials To Direct Stem-Cell Fate. *Nature* **2009**, *462*, 433−441.
(28) Ott, H. C.; Matthiesen, T. S.; Goh, S.-K.; Black, L. D.; Kren, S. M.; Netoff, T. I.; Taylor, D. A. Perfusion-Decellularized Matrix: Using Nature's Platform To Engineer a Bioartificial Heart. *Nat. Med.* **2008**, *14*, 213−221.
(29) Solanas, G.; Benitah, S. A. Regenerating the Skin: A Task for the Heterogeneous Stem Cell Pool and Surrounding Niche. *Nat. Rev. Mol. Cell Biol.* **2013**, *14*, 737−748.
(30) Dubois, S. G.; Floyd, E. Z.; Zvonic, S.; Kilroy, G.; Wu, X.; Carling, S.; Halvorsen, Y. D. C.; Ravussin, E.; Gimble, J. M. In *Mesenchymal Stem Cells*; Prockop, D. J., Bunnell, B. A., Phinney, D. G., Eds.; Springer: Berlin, Germany, 2008; Chapter 1, pp 69−79.
(31) Rasmussen, C.; Thomas-Virnig, C.; Allen-Hoffmann, B. L. In *Epithelial Cell Culture Protocols*; Randell, S. H., Fulcher, M. L., Eds.; Springer: Berlin, Germany, 2013; Chapter 11, pp 161−175.
(32) Picot, J. *Human Cell Culture Protocols*, 2nd ed.; Springer: Berlin, Germany, 2005.
(33) Freshney, R. I.; Stacey, G. N.; Auerbach, J. M. *Culture of Human Stem Cells*, 5th ed.; Wiley: Hoboken, NJ, 2007.
(34) Meluzzi, D.; Arya, G. Recovering Ensembles of Chromatin Conformations from Contact Probabilities. *Nucleic Acids Res.* **2013**, *41*, 63−75.
(35) Mirny, L. A. The Fractal Globule as a Model of Chromatin Architecture in the Cell. *Chromosome Res.* **2011**, *19*, 37−51.
(36) Plimpton, S. Fast Parallel Algorithms for Short-Range Molecular Dynamics. *J. Comput. Phys.* **1995**, *117*, 1−19.
(37) Wang, Z.; Wang, Y.; Farhangfar, F.; Zimmer, M.; Zhang, Y. Enhanced Keratinocyte Proliferation and Migration in Co-Culture with Fibroblasts. *PLoS One* **2012**, *7*, e40951.
(38) Deepa, R.; Paul, W.; Anilkumar, T.; Sharma, C. P. Differential Healing of Full Thickness Rabbit Skin Wound by Fibroblast Loaded Chitosan Sponge. *J. Biomater. Tissue Eng.* **2013**, *3*, 261−272.
(39) Bieling, P.; Laan, L.; Schek, H.; Munteanu, E. L.; Sandblad, L.; Dogterom, M.; Brunner, D.; Surrey, T. Reconstitution of a Microtubule Plus-End Tracking System in Vitro. *Nature* **2007**, *450*, 1100−1105.
(40) Ingber, D. E.; Prusty, D.; Sun, Z.; Betensky, H.; Wang, N. Cell Shape, Cytoskeletal Mechanics, and Cell Cycle Control in Angiogenesis. *J. Biomech.* **1995**, *28*, 1471−1484.
(41) Tan, K. Y.; Lin, H.; Ramstedt, M.; Watt, F. M.; Huck, W. T.; Gautrot, J. E. Decoupling Geometrical and Chemical Cues Directing Epidermal Stem Cell Fate on Polymer Brush-Based Cell Micro-Patterns. *Integr. Biol.* **2013**, *5*, 899−910.
(42) Gentile, F.; Tirinato, L.; Battista, E.; Causa, F.; Liberale, C.; Di Fabrizio, E. M.; Decuzzi, P. Cells Preferentially Grow on Rough Substrates. *Biomaterials* **2010**, *31*, 7205−7212.
(43) Schwartz, M. A.; DeSimone, D. W. Cell Adhesion Receptors in Mechanotransduction. *Curr. Opin. Cell Biol.* **2008**, *20*, 551−556.
(44) Fischer, R. S.; Myers, K. A.; Gardel, M. L.; Waterman, C. M. Stiffness-Controlled Three-Dimensional Extracellular Matrices for High-Resolution Imaging of Cell Behavior. *Nat. Protoc.* **2012**, *7*, 2056−66.
(45) McMurray, R.; Wann, A.; Thompson, C.; Connelly, J.; Knight, M. Surface Topography Regulates wnt Signaling through Control of Primary Cilia Structure in Mesenchymal Stem Cells. *Sci. Rep.* **2013**, *3*, 1−7.
(46) Baker, B. M.; Chen, C. S. Deconstructing the Third Dimension−How 3d Culture Microenvironments Alter Cellular Cues. *J. Cell Sci.* **2012**, *125*, 3015−3024.
(47) Kilian, K. A.; Bugarija, B.; Lahn, B. T.; Mrksich, M. Geometric Cues for Directing the Differentiation of Mesenchymal Stem Cells. *Proc. Natl. Acad. Sci. U.S.A.* **2010**, *107*, 4872−4877.
(48) Zhu, S.; Oh, H.-S.; Shim, M.; Sterneck, E.; Johnson, P. F.; Smart, R. C. C/Ebp$\beta$ Modulates the Early Events of Keratinocyte Differentiation Involving Growth Arrest and Keratin 1 and Keratin 10 Expression. *Mol. Cell. Biol.* **1999**, *19*, 7181−7190.
(49) Watt, F. M. Involucrin and Other Markers of Keratinocyte Terminal Differentiation. *J. Invest. Dermatol.* **1983**, *81*, 100s−103s.
(50) Saha, K.; Mei, Y.; Reisterer, C. M.; Pyzocha, N. K.; Yang, J.; Muffat, J.; Davies, M. C.; Alexander, M. R.; Langer, R.; Anderson, D. G. Surface-Engineered Substrates for Improved Human Pluripotent Stem Cell Culture under Fully Defined Conditions. *Proc. Natl. Acad. Sci. U.S.A.* **2011**, *108*, 18714−18719.
(51) Ahn, E. H.; Kim, Y.; An, S. S.; Afzal, J.; Lee, S.; Kwak, M.; Suh, K.-Y.; Kim, D.-H.; Levchenko, A. Spatial Control of Adult Stem Cell Fate Using Nanotopographic Cues. *Biomaterials* **2014**, *35*, 2401−2410.
(52) Yang, C.; Tibbitt, M. W.; Basta, L.; Anseth, K. S. Mechanical Memory and Dosing Influence Stem Cell Fate. *Nat. Mater.* **2014**, *13*, 645−652.
(53) Ingber, D. E. Mechanical Control of Tissue Growth: Function Follows Form. *Proc. Natl. Acad. Sci. U.S.A.* **2005**, *102*, 11571−11572.
(54) McBeath, R.; Pirone, D. M.; Nelson, C. M.; Bhadriraju, K.; Chen, C. S. Cell Shape, Cytoskeletal Tension, and Rhoa Regulate Stem Cell Lineage Commitment. *Dev. Cell* **2004**, *6*, 483−495.
(55) Wang, N.; Tytell, J. D.; Ingber, D. E. Mechanotransduction at a Distance: Mechanically Coupling the Extracellular Matrix with the Nucleus. *Nat. Rev. Mol. Cell Biol.* **2009**, *10*, 75−82.
(56) Mercurio, F.; Manning, A. M. Nf-Kb as a Primary Regulator of the Stress Response. *Oncogene* **1999**, *18*.
(57) Cremer, T.; Cremer, C. Chromosome Territories, Nuclear Architecture and Gene Regulation in Mammalian Cells. *Nat. Rev. Genet.* **2001**, *2*, 292−301.

(58) Yabuki, M.; Miyake, T.; Fujiwara, T.; Hamazaki, K.; Yoshioka, T.; Horton, A.; Utsumi, K. Role of Nuclear Lamins in Nuclear Segmentation of Human Neutrophils. *Physiol. Chem. Phys. Med. NMR* **1998**, *31*, 77−84.
(59) Hoffmann, K.; Sperling, K.; Olins, A. L.; Olins, D. E. The Granulocyte Nucleus and Lamin B Receptor: Avoiding the Ovoid. *Chromosoma* **2007**, *116*, 227−235.
(60) Pajerowski, J. D.; Dahl, K. N.; Zhong, F. L.; Sammak, P. J.; Discher, D. E. Physical Plasticity of the Nucleus in Stem Cell Differentiation. *Proc. Natl. Acad. Sci. U.S.A.* **2007**, *104*, 15619−15624.
(61) Parada, L. A.; McQueen, P. G.; Misteli, T. Tissue-Specific Spatial Organization of Genomes. *Genome Biol.* **2004**, *5*, R44.
(62) Lieberman-Aiden, E.; van Berkum, N. L.; Williams, L.; Imakaev, M.; Ragoczy, T.; Telling, A.; Amit, I.; Lajoie, B. R.; Sabo, P. J.; Dorschner, M. O. Comprehensive Mapping of Long-Range Interactions Reveals Folding Principles of the Human Genome. *Science* **2009**, *326*, 289−293.
(63) Fletcher, D. A.; Mullins, R. D. Cell Mechanics and the Cytoskeleton. *Nature* **2010**, *463*, 485−492.
(64) Strambio-De-Castillia, C.; Niepel, M.; Rout, M. P. The Nuclear Pore Complex: Bridging Nuclear Transport and Gene Regulation. *Nat. Rev. Mol. Cell Biol.* **2010**, *11*, 490−501.
(65) Lammerding, J.; Fong, L. G.; Ji, J. Y.; Reue, K.; Stewart, C. L.; Young, S. G.; Lee, R. T. Lamins A and C but Not Lamin B1 Regulate Nuclear Mechanics. *J. Biol. Chem.* **2006**, *281*, 25768−25780.
(66) Constantinescu, D.; Gray, H. L.; Sammak, P. J.; Schatten, G. P.; Csoka, A. B. Lamin A/C Expression Is a Marker of Mouse and Human Embryonic Stem Cell Differentiation. *Stem Cells* **2006**, *24*, 177−185.
(67) Isermann, P.; Lammerding, J. Nuclear Mechanics and Mechanotransduction in Health and Disease. *Curr. Biol.* **2013**, *23*, R1113−R1121.
(68) Jamali, Y.; Azimi, M.; Mofrad, M. R. A Sub-Cellular Viscoelastic Model for Cell Population Mechanics. *PLoS One* **2010**, *5*, e12097.
(69) Fudenberg, G.; Getz, G.; Meyerson, M.; Mirny, L. A. High Order Chromatin Architecture Shapes the Landscape of Chromosomal Alterations in Cancer. *Nat. Biotechnol.* **2011**, *29*, 1109−1113.
(70) Humphrey, W.; Dalke, A.; Schulten, K. VMD: Visual Molecular Dynamics. *J. Mol. Graphics* **1996**, *14*, 33−38.